Measurement Science and Technology

PAPER

Multisensor signal denoising based on matching synchrosqueezing wavelet transform for mechanical fault condition assessment

To cite this article: Cancan Yi *et al* 2018 *Meas. Sci. Technol.* **29** 045104

IOP Publishing Measurement Science and Technology
Meas. Sci. Technol. **29** (2018) 045104 (15pp) https://doi.org/10.1088/1361-6501/aaa50a

Multisensor signal denoising based on matching synchrosqueezing wavelet transform for mechanical fault condition assessment

Cancan Yi[1,2,3]**, Yong Lv**[2,3]**, Han Xiao**[2,3]**, Tao Huang**[2,3] **and Guanghui You**[4]

[1] Engineering Research Center for Metallurgical Automation and Measurement Technology of Ministry of Education, Wuhan University of Science and Technology, Wuhan 430081, People's Republic of China
[2] Key Laboratory of Metallurgical Equipment and Control Technology, Wuhan University of Science and Technology, Ministry of Education, Wuhan 430081, People's Republic of China
[3] Hubei Key Laboratory of Mechanical Transmission and Manufacturing Engineering, Wuhan University of Science and Technology, Wuhan 430081, People's Republic of China
[4] Zhejiang Institute of Mechanical & Electrical Engineering, Hangzhou 310053, People's Republic of China

E-mail: lvyong@wust.edu.cn

Received 10 September 2017, revised 19 December 2017
Accepted for publication 4 January 2018
Published 6 March 2018

Abstract

Since it is difficult to obtain the accurate running status of mechanical equipment with only one sensor, multisensor measurement technology has attracted extensive attention. In the field of mechanical fault diagnosis and condition assessment based on vibration signal analysis, multisensor signal denoising has emerged as an important tool to improve the reliability of the measurement result. A reassignment technique termed the synchrosqueezing wavelet transform (SWT) has obvious superiority in slow time-varying signal representation and denoising for fault diagnosis applications. The SWT uses the time–frequency reassignment scheme, which can provide signal properties in 2D domains (time and frequency). However, when the measured signal contains strong noise components and fast varying instantaneous frequency, the performance of SWT-based analysis still depends on the accuracy of instantaneous frequency estimation. In this paper, a matching synchrosqueezing wavelet transform (MSWT) is investigated as a potential candidate to replace the conventional synchrosqueezing transform for the applications of denoising and fault feature extraction. The improved technology utilizes the comprehensive instantaneous frequency estimation by chirp rate estimation to achieve a highly concentrated time–frequency representation so that the signal resolution can be significantly improved. To exploit inter-channel dependencies, the multisensor denoising strategy is performed by using a modulated multivariate oscillation model to partition the time–frequency domain; then, the common characteristics of the multivariate data can be effectively identified. Furthermore, a modified universal threshold is utilized to remove noise components, while the signal components of interest can be retained. Thus, a novel MSWT-based multisensor signal denoising algorithm is proposed in this paper. The validity of this method is verified by numerical simulation, and experiments including a rolling bearing system and a gear system. The results show that the proposed multisensor matching synchronous squeezing wavelet transform (MMSWT) is superior to existing methods.

Keywords: multisensor signal analysis, matching synchrosqueezing transform, wavelet denoising, fault diagnosis

(Some figures may appear in colour only in the online journal)

1. Introduction

A variety of equipment in the metallurgical industry, such as converter tilting mechanisms and ladle rotary tables, play unique and important roles in production processes. Since such equipment normally works over a long term in environments with high temperature and high humidity, and withstanding heavy workload, the mechanical components of the equipment may be damaged during operation. An equipment accident will seriously affect production efficiency, and cause serious economic losses. Therefore, state monitoring of running equipment based on vibration measurement and signal analysis techniques has vital significance to ensure safety [1, 2]. There is no doubt that signal processing is an important part of measurement science. Our goal is to improve the signal-to-noise ratio of the measured signals and achieve accurate identification of fault characteristics. Existing signal processing methods, such as detrended fluctuation analysis [3], have some limitations in dealing with the nonlinear and non-stationary fault signal. Some advanced signal processing methods, such as the synchrosqueezing transform, have attracted much attention in denoising [4].

Currently, there are two kinds of signal processing methods that arouse the interest of many researchers. One is adaptive decomposition methods based on data-driven techniques, such as empirical mode decomposition (EMD) [5]. The other kind is frequency redistribution methods, such as the synchrosqueezing transform [6, 7], whose core idea is to shift the time frequency distribution to the center of the energy in the time–frequency plane. Although the most representative adaptive decomposition algorithm, EMD and its modified version have some disadvantages, like modal aliasing and the end effect [8, 9]. Instantaneous frequency describes the rapid oscillation characteristics of a vibration signal in a continuous time span [10]. Therefore, accurate estimation of the instantaneous frequency is important research in the field of structural states monitoring and fault diagnosis. Conventional time–frequency analysis methods, including the short-time Fourier transform [11], wavelet transform [12], and Wigner Ville distribution [13], always result in obscure time–frequency representation. To solve this problem, Daubechies *et al* [14] proposed the synchrosqueezing wavelet transform (SWT), which belongs to a time–frequency rearrangement algorithm [15]. This method aims to improve the time–frequency distribution of aggregation in the scale domain and reduce the distortion of the instantaneous frequency curve. Most importantly, it supports signal reconstruction and offers better readability, namely time–frequency resolution. Since the SWT has a more solid mathematical foundation than EMD, it is more suitable for the early fault diagnosis of key equipment components under complicated measurement environments, such as strong noise interference [16].

A variety of new methods based on synchronous transformation have been proposed, such as synchronous S-transform [17], second-order synchrosqueezing transform (SST) [18], and synchronous wavelet packet transform [19]. However, the existing SST methods follow the assumption that the signal has a slow time-varying instantaneous frequency, and the reassignment is based on the instantaneous frequency estimation. Essentially, it is a zero-order estimation of the true instantaneous frequency. Actually, these methods perform unexpectedly. Hence, an improved SWT, namely the matching synchrosqueezing wavelet transform (MSWT), was investigated to achieve a highly concentrated time–frequency representation, even for signals with strong noise components. A zero-order instantaneous frequency estimation was employed in the original SWT. Conversely, the MSWT was proposed with a high-order estimation by incorporating the instantaneous frequency estimation and group delay estimation, which transformed the chirp rate estimation into a comprehensive and accurate time–frequency representation [20]. Therefore, the MSWT had better performance in feature frequency identification.

Facing feature information recognition, it is commonly accepted that multisensor information fusion technology has better performance than traditional signal processing using a single sensor. In the domain of multisensor signal processing, Aminghafari *et al* [21] firstly proposed the multivariate wavelet denoising (MWD) algorithm, and carried out principal component analysis (PCA) on the detail coefficient matrix to determine the universal threshold of noise removal. However, the noise component has an obvious influence on matrix decomposition results, and the correlation between the multi-channels could not be fully considered. Subsequently, research has focused on bivariate empirical mode decomposition [22], trivariate empirical mode decomposition [23], and multivariate empirical mode decomposition [24]. However, the adopted high-dimensional uniform sampling strategy is not able to reflect the high-dimensional distribution characteristics of the collected data. Meanwhile, there are some deficiencies in the decomposition ability of the complex noisy signal. One study used quaternion singular spectrum analysis to couple four-channel signals [25]. However, the requisite four-channel signal is a special case, and it cannot meet the needs of reality. Distinguished from traditional univariate denoising methods, the multivariate denoising approach is more complex. Recently, multivariate wavelet synchrosqueezing denoising (MWSD) was proposed for float drift denoising [26, 27]. This could be achieved by partitioning the time–frequency domain, which aims to identify a set of common modulated oscillations to the multisensor data. The notion of the modulated

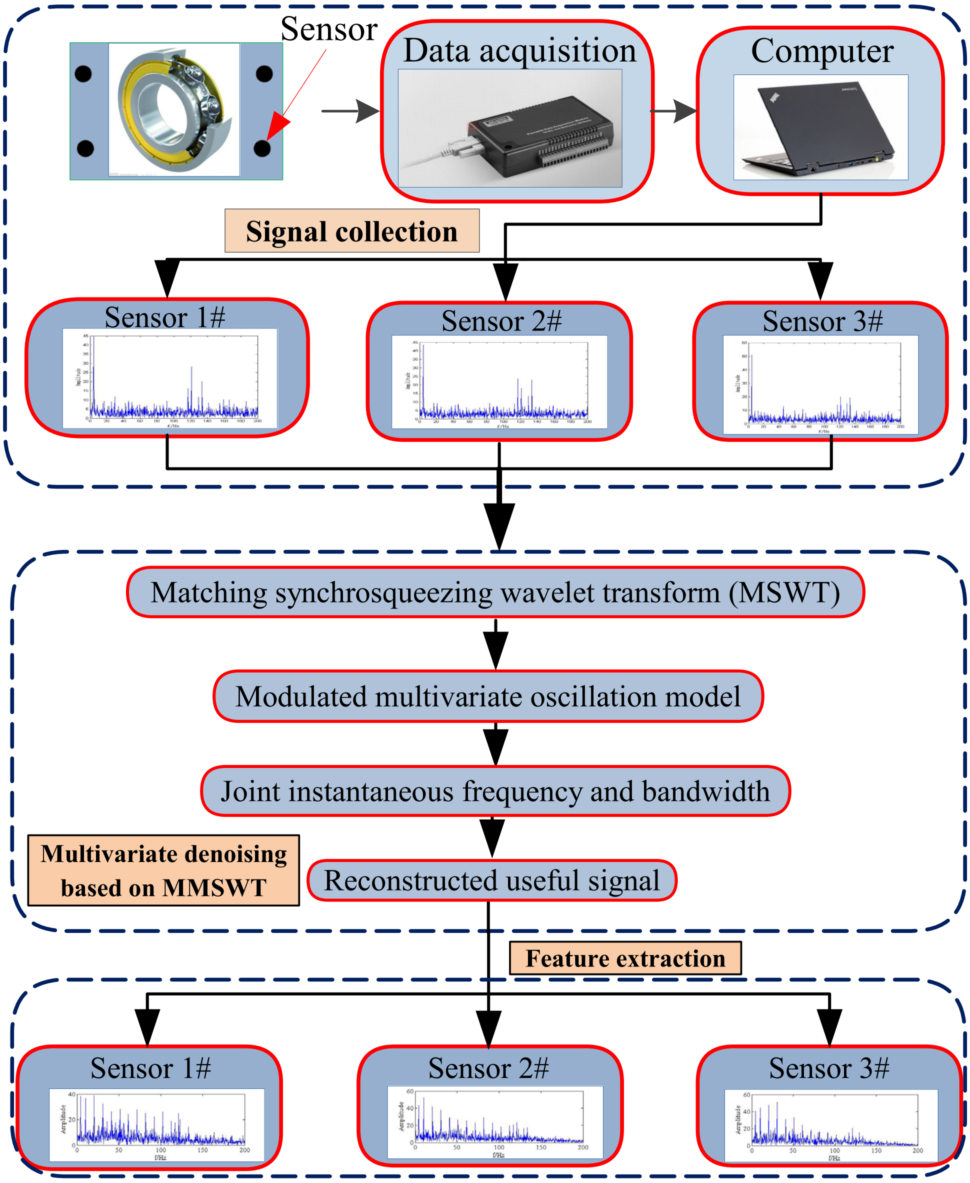

Figure 1. Flowchart of the proposed method for fault diagnosis.

multivariate oscillation has been introduced in [28], where modulated oscillations in multiple channels were modeled by a single oscillatory structure. The results demonstrated that the synchrosqueezing transform theory can be regarded as a powerful tool in dealing with noisy multisensor data.

In this paper, an improved multisensor signal denoising algorithm based on the matching synchroqueezing wavelet transform and modulated multivariate oscillation model, i.e. a multisensor matching synchronous squeezing wavelet transform (MMSWT), is proposed and well-studied. The improved method utilizes the comprehensive and accurate high-order instantaneous frequency estimation to replace the instantaneous frequency estimation in the MWSD method described in [26]. The structure of this paper is as follows: in section 2, the properties of the MSWT and the multisensor signal denoising method based on the modulated multivariate oscillation model are briefly introduced. Then, it focuses on the proposed multisensor denoising algorithm. In sections 3–5, the numerical simulated signal (section 3) and experimental signal (sections 4 and 5) collected from a damaged rolling bearing system are analyzed using the proposed algorithm to verify the validity of the method. Our conclusions are summarized in section 5.

2. Proposed method

2.1. MSWT [20]

The synchrosqueezing transform of a signal is based on the wavelet transform. Given the measured signal $x(t)$, the continuous wavelet transform [29] can be expressed as follows:

$$W_x^{\psi}(a,b) = \int a^{-1/2}\psi^*\left(\frac{t-b}{a}\right)x(t)\mathrm{d}t, \tag{1}$$

where a denotes the scale factor, b is the shift factor, $\psi(t)$ represents the mother wavelet function, and $\psi^*(t)$ is corresponding to complex conjugate operator to $\psi(t)$. Essentially,

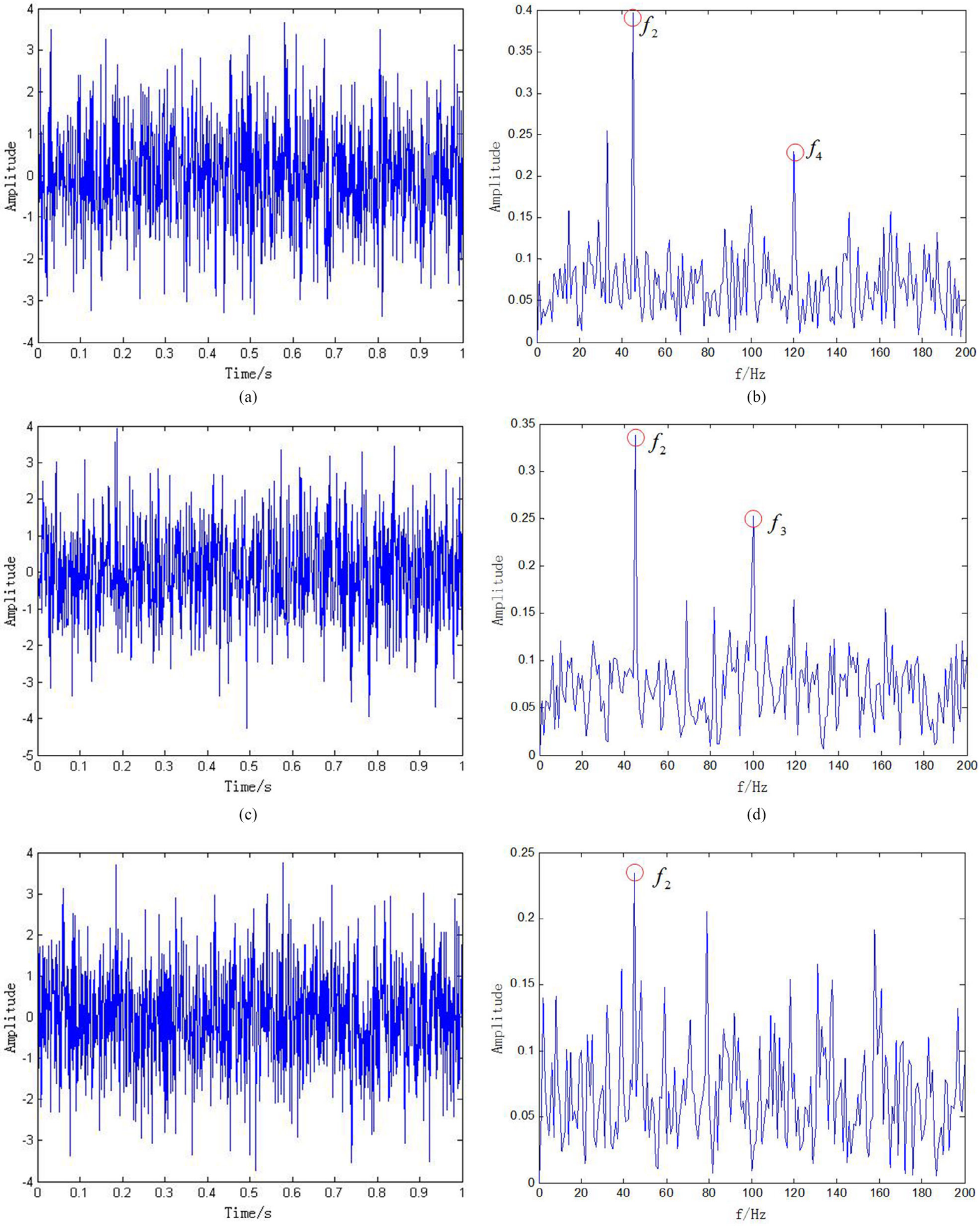

Figure 2. Time and frequency responses of the three-sensor numerical simulation signal. (a) Signal of the first sensor in the time domain. (b) Signal of the first sensor in the frequency domain. (c) Signal of the second sensor in the time domain. (d) Signal of the second sensor in the frequency domain. (e) Signal of the third sensor in the time domain. (f) Signal of the third sensor in the frequency domain.

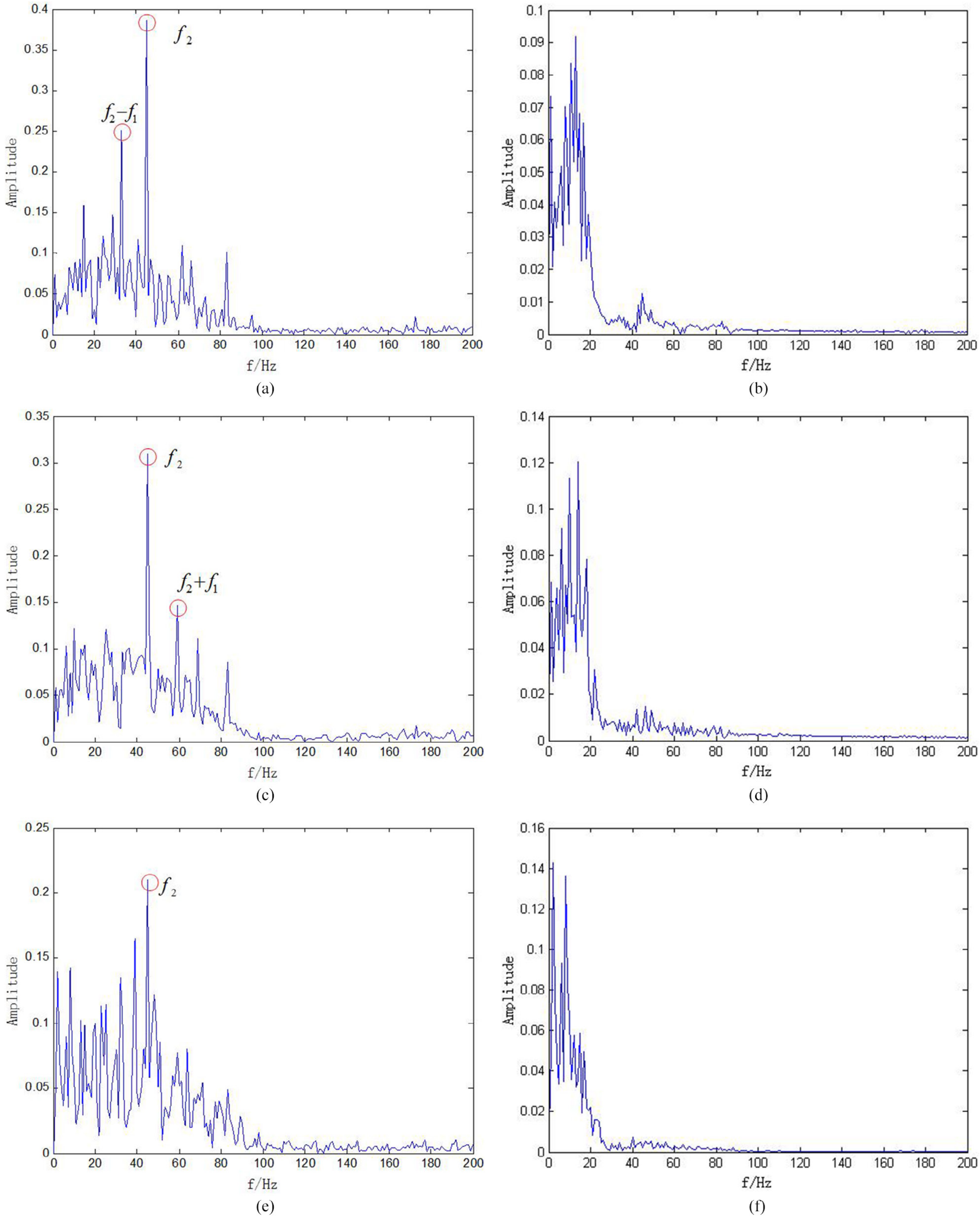

Figure 3. Comparison of the denoising performance of the simulation signal between MWSD (figures (a), (c) and (e)) and MWD (figures (b), (d) and (f)). (a) Signal of the first sensor denoised by MWSD. (b) Signal of the first sensor denoised by MWD. (c) Signal of the second sensor denoised by MWSD. (d) Signal of the second sensor denoised by MWD. (e) Signal of the third sensor denoised by MWSD. (f) Signal of the third sensor denoised by MWD.

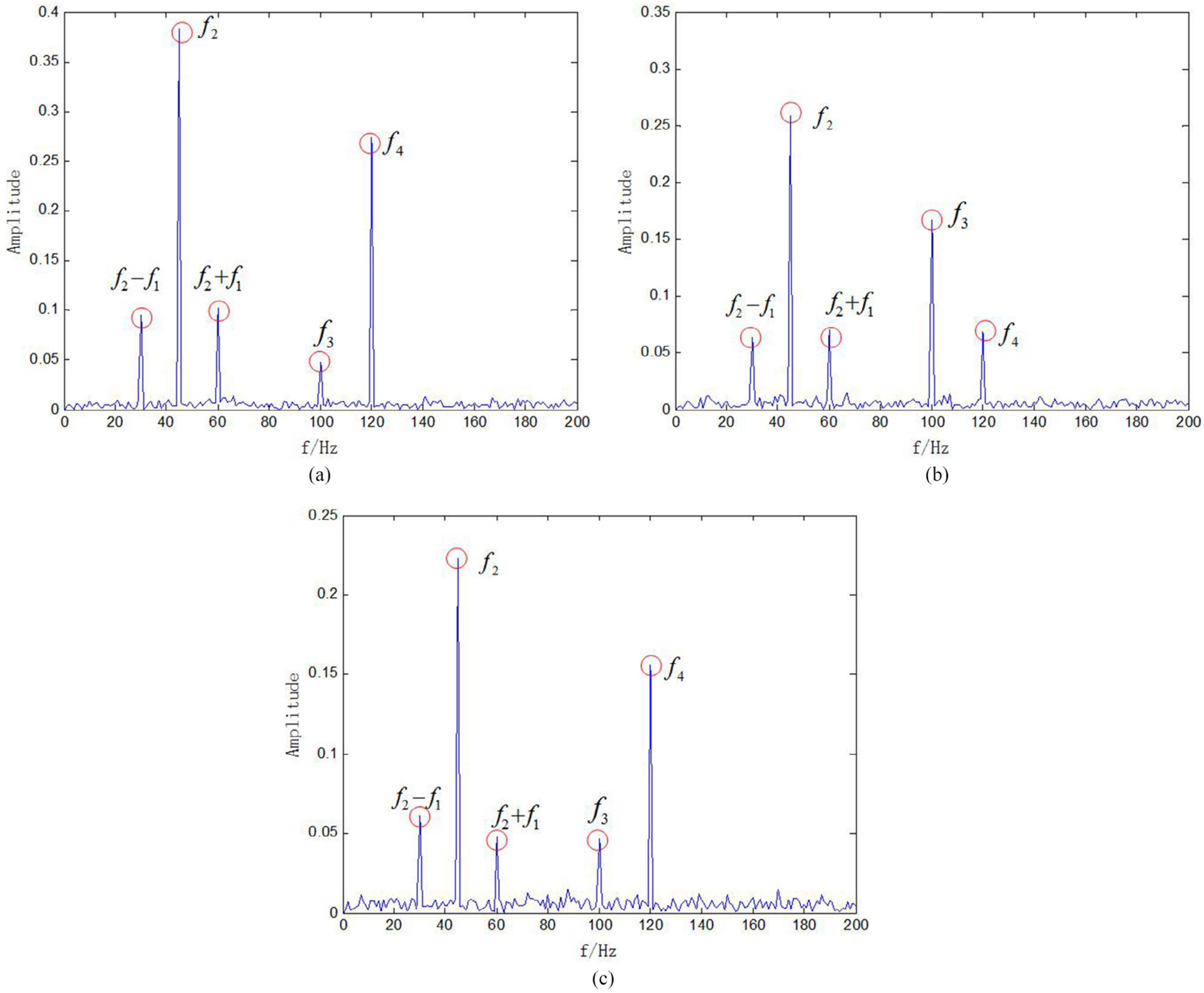

Figure 4. Results computed by the MMSWT. (a) Signal of the first sensor denoised by the MMSWT. (b) Signal of the second sensor denoised by the MMSWT. (c) Signal of the third sensor denoised by the MMSWT.

$W_x^{\psi}(a,b)$ is provided by inner production between the analysis signal and the wavelet function. It should also be noted that for different scale factors there are some overlaps among wavelet filters. For instance, given a single harmonic signal with a frequency w, if the primary frequency of the mother wavelet is w_0, the wavelet coefficients should be theoretically concentrated in the location $a = w_0/w$. However, the actual wavelet coefficients are often diffused in the scale direction, and cannot be focused as expected, and thus the time–frequency graph becomes fuzzy. Therefore, an estimation of the instantaneous frequency $w_x(a,b)$ for each scale–time pair (a,b) can be calculated as in [30]:

$$w_x(a,b) = -\mathrm{i}W_x^{\psi}(a,b)^{-1}\frac{\partial W_x^{\psi}(a,b)}{\partial b}, \qquad (2)$$

where $\mathrm{i} = \sqrt{-1}$ is the imaginary unit. By calculating the instantaneous frequency, the time–scale plane (b,a) can be mapped into the time–frequency plane $(b, w_x(a,b))$ in order to realize a sharpened time–frequency representation, which is the basic idea of the SWT [14]. Then, the SWT can be expressed as follows:

$$T(w,b) = \int W_x^{\psi}(a,b)a^{-3/2}\delta(w_x(a,b) - w)\mathrm{d}a, \qquad (3)$$

where $\delta(\bullet)$ is the Dirac function. Since the SWT is the rearrangement of the complex wavelet coefficients in the frequency domain, it is reversible and applicable for signal reconstruction. The traditional SWT has certain advantages for stationary signal analysis; however, the vibration signals of rolling mills and aircraft engines have non-stationary and nonlinear characteristics. Taking this into consideration, a novel MSWT method [20] that can realize the energy rearrangement in the scale direction and ignore the change in time, is introduced in this paper. Firstly, the time–frequency estimation, group delay estimation, and linear frequency modulation estimation are defined, respectively, as follows:

$$\tilde{w}_x(a,b) = \frac{\partial_b W_x^{\psi}(a,b)}{\mathrm{i}W_x^{\psi}(a,b)} \qquad (4)$$

$$\tilde{t}_x(a,b) = b + \frac{aW_x^{t\,\psi}(a,b)}{W_x^{\psi}(a,b)} \tag{5}$$

$$\tilde{c}_x(a,b) = \frac{\partial_b \tilde{w}_x(a,b)}{\partial_b \tilde{t}_x(a,b)}. \tag{6}$$

Based on the three estimations described in equations (4)–(6), the new instantaneous frequency estimation based on linear frequency modulation is expressed as follows:

$$\tilde{w}_x^m(a,b) = \tilde{w}_x(a,b) + \tilde{c}_x(a,b)[b - \tilde{t}_x(a,b)]. \tag{7}$$

Based on the definition of instantaneous frequency estimation in equation (7), the rapid change of the vibration signal can be better matched in the time–frequency structure. Thus, the MSWT based on the rearrangement of the linear frequency modulation process [31] is defined as in the following expression:

$$T_x^m(w,b) = \int W_x^{\psi}(a,b)a^{-3/2}\delta(w - \tilde{w}_x^m(a,b))\mathrm{d}a. \tag{8}$$

The difference between the introduced MSWT and the original SWT is that the time–frequency estimation in the SWT is replaced by the new instantaneous frequency estimation defined by equation (7). The synchrosqueezing transform rearrangement information (b,a) is redistributed to $(b, \tilde{w}_x^m(a,b))$. The MSWT based on linear frequency modulation inherits the basic idea of time–frequency analysis while simultaneously considering the time and scale variables. The definition of instantaneous frequency estimation given in equation (7) is the high-level estimation of the instantaneous frequency. Meanwhile, even for the signal with rapidly changing instantaneous frequency, the concentrated time–frequency expression can also be realized to avoid interference from cross terms.

2.2. A joint scheme for multivariate signal denoising

We can define a multisensor signal $\boldsymbol{X}(t)$ with N sensors as follows:

$$\boldsymbol{X}(t) = \begin{bmatrix} a_1(t)\mathrm{e}^{\mathrm{i}\phi_1(t)} \\ a_2(t)\mathrm{e}^{\mathrm{i}\phi_2(t)} \\ \vdots \\ a_N(t)\mathrm{e}^{\mathrm{i}\phi_N(t)} \end{bmatrix}, \tag{9}$$

where a_n and ϕ_n represent the instantaneous amplitude and phase, respectively, for each sensor index n. It is worth mentioning that the variable n varies from 1 to N.

Subsequently, the MSWT is applied to signals collected by each sensor, and then the corresponding synchrosqueezing wavelet coefficients can be defined as $T_n(w,b)$ $(n = 1, ..., N)$. To capture the common sensor-wise characteristics, the multivariate modulated oscillation model is employed to determine the joint instantaneous frequency and multivariate bandwidth. Firstly, the initial joint instantaneous frequency $w_x(t)$ is computed based on the modulated oscillations model [28]:

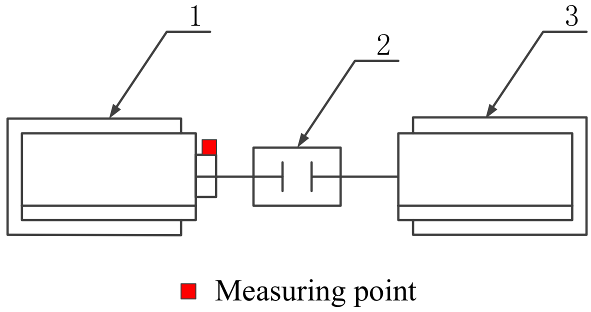

Figure 5. Schematic diagram.

$$w_x(t) = \frac{\Im\left\{X^H(t)\frac{\mathrm{d}}{\mathrm{d}t}X(t)\right\}}{\|X(t)\|^2} = \frac{\sum_{n=1}^N a_n^2(t)\phi_n'(t)}{\sum_{n=1}^N a_n^2(t)}. \tag{10}$$

The joint analytic spectrum corresponding to a multivariate signal is expressed as

$$S_x(w) = \frac{1}{E}\|F_x(w)\|^2, \tag{11}$$

where $F_x(\bullet)$ denotes the Fourier transform for every single sensor signal, and the energy of the joint analysis spectrum is $E = \frac{1}{2\pi}\int \|F_x(w)\|^2\mathrm{d}w$. The next step is to calculate the squared multivariate bandwidth by

$$B_x^2 = \frac{1}{2\pi}\int_0^{\infty}(w - \bar{w}_x)^2 S_x(w)\mathrm{d}w, \tag{12}$$

where $\bar{w}_x = \frac{1}{2\pi}\int wS_x(w)\mathrm{d}w$ is the joint global mean frequency.

Then, the joint instantaneous frequency $w_x(t)$ is divided in the time–frequency domain into 2^l equal width frequency bands. Each frequency band is expressed as

$$w_{l,m} = \left[\frac{m}{2^{l+1}}, \frac{m+1}{2^{l+1}}\right], \tag{13}$$

where $l = 0, ..., L_s$ is the level of the frequency bands, and $m = 0, ..., 2^l - 1$ is the index of the frequency bands. Then, the multivariate bandwidth $B_{l,m}$ can be calculated from the given frequency bands $w_{l,m}$ according to equation (12). It should be pointed out that $w_{l,m}$ splits into two frequency sub-bands $w_{l+1,2m}$ and $w_{l+1,2m+1}$ on the condition that $B_{l,m} > B_{l+1,2m} + B_{l+1,2m+1}$. According to the modulated multivariate oscillation model, the modulated oscillations in multisensor and inter-sensor dependencies are obtained by partitioning the time–frequency domain into a set of frequency bands $\{w_v\}$ $(v = 1, ..., V)$, where V is the number of oscillatory scales, and $w_1 > w_2 > \cdots > w_V$. For a multisensor signal $\boldsymbol{X}(t)$, the corresponding partitioned MSWT coefficients $F_{n,v}(w,b)$ can be expressed as follows:

$$F_{n,v}(w,b) = \sum_{w\in w_v} T_n(w,b), \tag{14}$$

Table 1. Experiment parameters and failure frequency of bearing.

Rotation speed (r min^{-1})	Rotation frequency(Hz)	Sampling frequency(Hz)	Outer race fault frequency (Hz)
1500	25	97 656	80

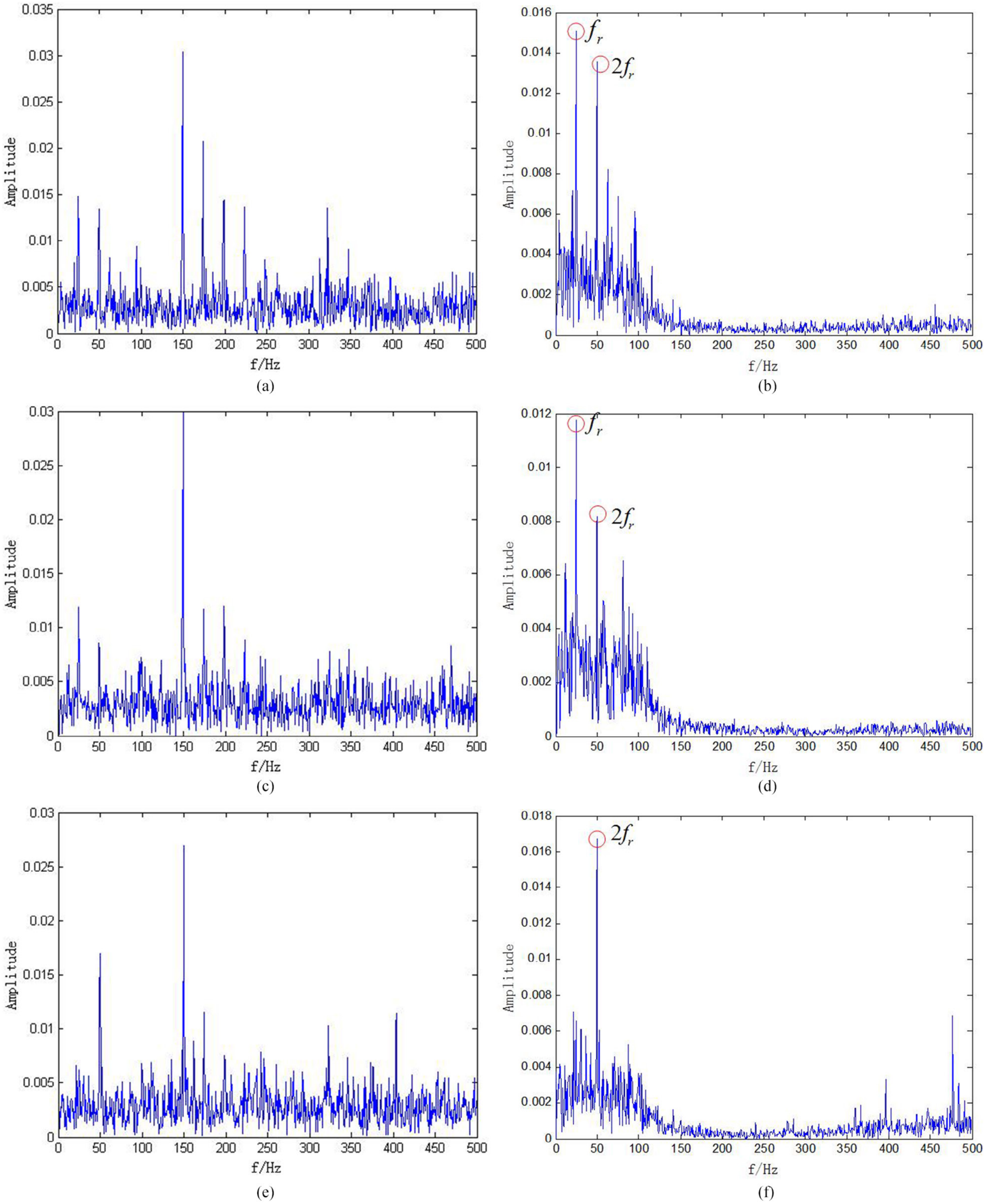

Figure 6. Frequency spectra of the original signal (figures (a), (c) and (e)) and the denoised result obtained by MWD (figures (b), (d) and (f)). (a) Frequency response of original signal in the *X*-scale. (b) Denoised signal of the *X*-scale by MWD. (c) Frequency response of original signal in the *Y*-scale. (d) Denoised signal of the *Y*-scale by MWD. (e) Frequency response of original signal in the *Z*-scale. (f) Denoised signal of the *Z*-scale by MWD.

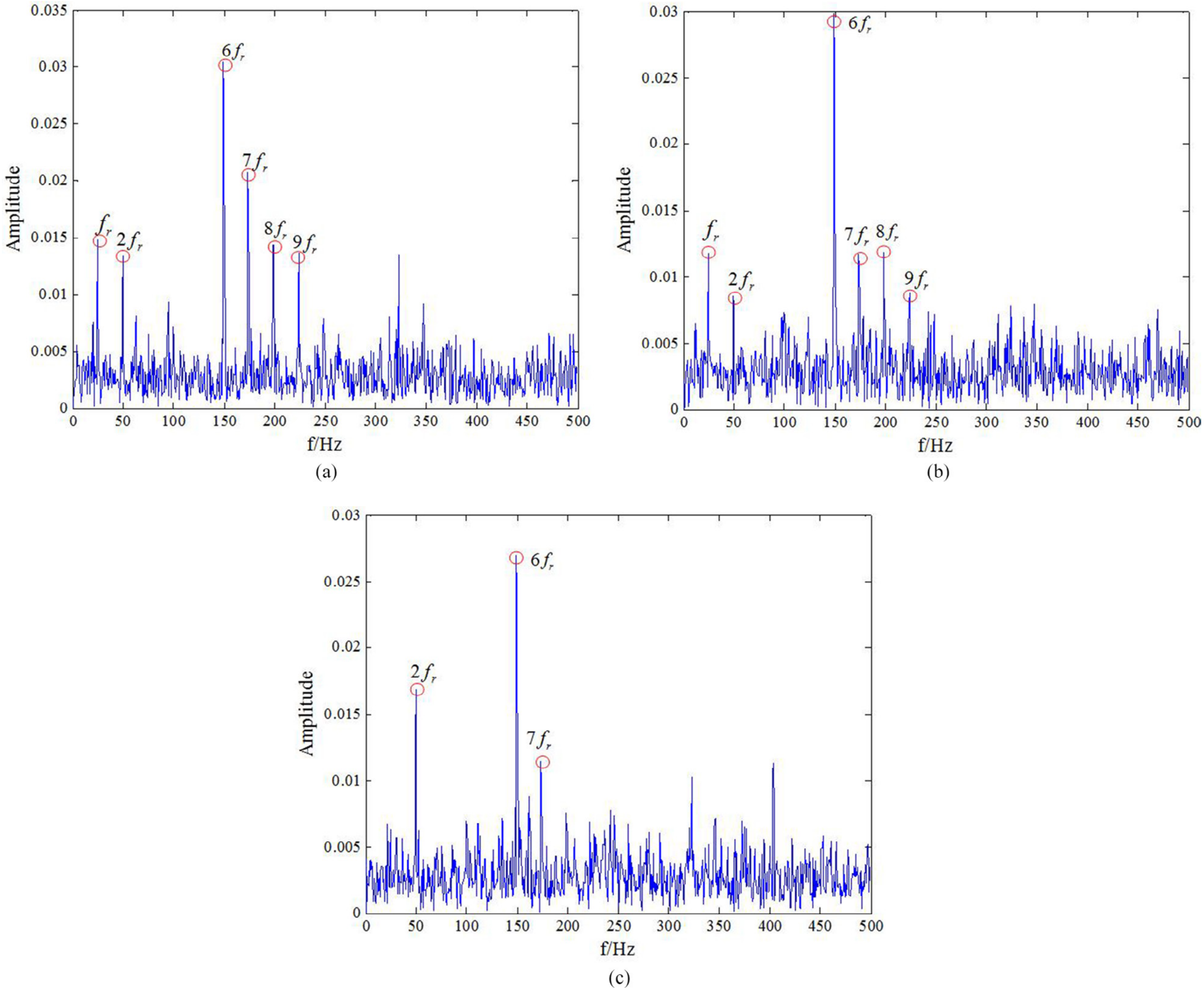

Figure 7. Denoising result of three-axis sensor computed by MWSD. (a) Denoised signal of the *X*-scale by MWSD. (b) Denoised signal of the *Y*-scale by MWSD. (c) Denoised signal of the *Z*-scale by MWSD.

where n indicates the sensor index, and v represents the oscillatory scale. Then, the multisensor signal denoising algorithm is performed by a thresholding technique that employs the multivariate instantaneous amplitude as follows:

$$\overset{\Lambda}{F}_{n,v}(w,b) = \begin{cases} F_{n,v}(w,b), & A_v^{\text{multi}}(w,b) > T_{\text{mod}} \\ 0, & A_v^{\text{multi}}(w,b) \leqslant T_{\text{mod}} \end{cases}, \quad (15)$$

where $A_v^{\text{multi}}(w,b) = \sqrt{\sum_{n=1}^{N} |F_{n,v}(w,b)|^2}$, and T_{mod} is the modified universal threshold (typically 0.1–0.3) [30]. Ultimately, the reconstruction signal $\overset{\Lambda}{S}_n(b)$ can be computed by an inverse transformation to the coefficients $\overset{\Lambda}{F}_{n,v}(b)$ as follows:

$$S_n^{\Lambda}(b) = \Re\left\{ C_\psi^{-1} \sum_{v=1}^{V} \int_{-\infty}^{+\infty} \overset{\Lambda}{F}_{n,v}(b)(w,b)\mathrm{d}w \right\}, \quad (16)$$

where $C_\psi = \int_{-\infty}^{+\infty} \overline{\psi(w)} w^{-1}\mathrm{d}w$, and $\Re(\centerdot)$ is the real part of the complex number.

2.3. Procedure of the proposed method

A flowchart of our proposed method for mechanical fault diagnosis is shown in figure 1.The detailed algorithm is described as follows.

(1) Given a multisensor signal $\boldsymbol{X}(t)$ with N sensors, the MSWT is applied to the sensor-wise characteristics, and the synchrosqueezing wavelet coefficient $T_n(w,b)$ is obtained.
(2) According to multivariate bandwidth, the joint instantaneous frequency $w_{l,m}$ is partitioned into a set of frequency bands $\{w_v\}$ $(v = 1, ..., V)$. Thus, the coefficient $T_n(w,b)$ is separated into oscillatory components $F_{n,v}(b)$.

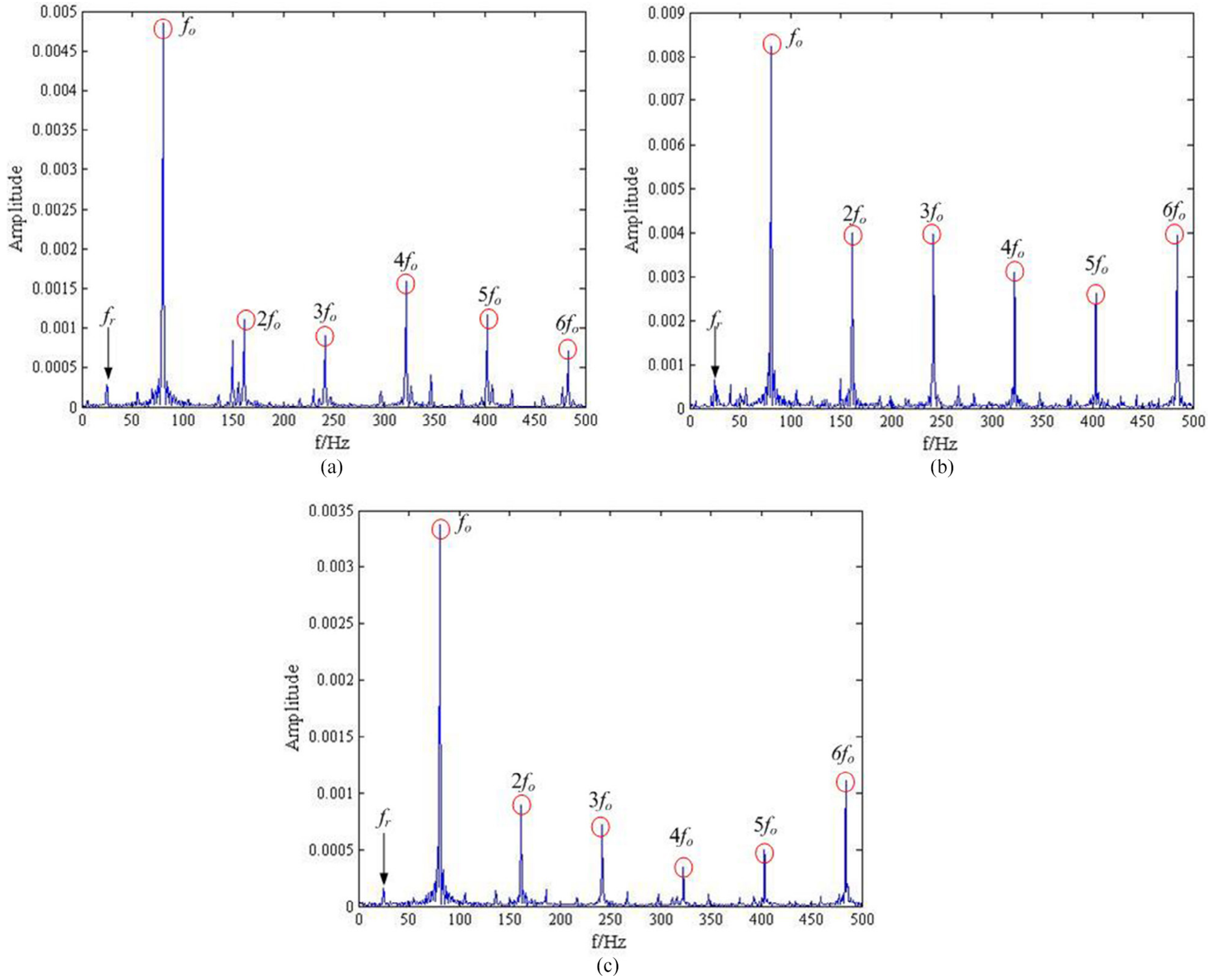

Figure 8. Denoising result of three-axis sensor computed by the MMSWT. (a) Denoised signal of the *X*-scale by the MMSWT. (b) Denoised signal of the *Y*-scale by the MMSWT. (c) Denoised signal of the *Z*-scale by the MMSWT.

(3) The multivariate instantaneous amplitude $A_v^{\text{multi}}(b)$ and universal threshold T_{mod} are calculated, respectively.
(4) The signal denoising process is conducted by equation (15), and the expected reconstruction signal is obtained by equation (16).

3. Numerical simulation analyses

Without loss of generality, first, the numerical analysis is performed to demonstrate the performance of the proposed method in multisensor signal processing. The mechanical failure signal is commonly composed of three parts: the modulation signal, harmonic signal, and noise components. The simulation signal model is expressed as below.

$$x_1 = 0.5(1 + 0.5\cos(2\pi f_1 t))\sin(2\pi f_2 t) \tag{17}$$

$$x_2 = 0.3\cos(2\pi f_3 t + 10) \tag{18}$$

$$x_3 = 0.2\sin(2\pi f_4 t - 15). \tag{19}$$

Here, $f_1 = 15$ Hz, $f_2 = 45$ Hz, $f_3 = 100$ Hz, and $f_4 = 120$ Hz. The sampling point is 1024, and the sampling frequency is 1024 Hz. In order to simulate a multisensor testing system, three source signals $\boldsymbol{X} = [x_1, x_2, x_3]$ are simultaneously collected by three sensors. It is the case that each of the measured signals is a mixture of the source signal. The noise components will be collected simultaneously, and thus Gaussian white noise is added to simulate the real situation. To randomly mix the three simulated source signals, a random matrix ($\boldsymbol{A}$) is optionally employed as follows:

$$\boldsymbol{A} = \begin{bmatrix} 0.2216 & 0.7252 & 0.2021 \\ 0.2040 & 0.8344 & 0.4691 \\ 0.6241 & 0.0189 & 0.3784 \end{bmatrix}. \tag{20}$$

Then, the simulated collected signal $\boldsymbol{Y}$ can be obtained by

$$\boldsymbol{Y} = \boldsymbol{AX} + \boldsymbol{N}, \tag{21}$$

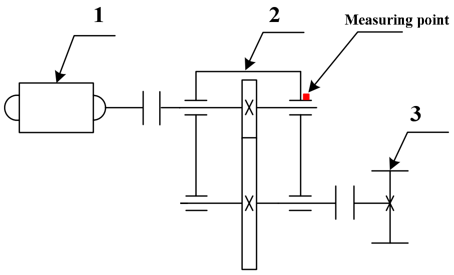

1- Magnetic powder brake, 2-Single stage gear transmission, 3- Variable speed drive

(a)

(b)

Figure 9. A gear system with a broken tooth. (a) System structure diagram. (b) Picture of the real device.

where $\boldsymbol{Y} = [y_1, y_2, y_3]$, and $\boldsymbol{N}$ is the Gaussian white noise corresponding to three sensors with a variance of 1.2. The time and frequency response about the collected signal $\boldsymbol{Y}$ is plotted in figure 2.

As observed from figure 2, the modulation feature can hardly be identified, and the characteristic frequency corresponding to the harmonic signal is also interfered by other signal components. For instance, only the feature frequencies f_2 and f_4 have been extracted from the simulation signal of the first sensor. Hence, the traditional fast Fourier transform (FFT) method is unsuitable for feature extraction of complex signals with strong noise. Undoubtedly, the optimal outcome is all the signal components including modulation and harmonic features, both of which can be inspected. Then, conventional methods, such as MWSD and MWD, are applied for simulation signal analysis, and the results are plotted in figure 3. Figures 3(a), (c) and (e) depict the denoising result provided by MWSD, and figures 3(b), (d) and (f) show the result computed by MWD. Although the feature frequency f_2 can be clearly identified in figures 3(a), (c) and (e), other harmonic frequencies such as f_3 and f_4 are still submerged. Moreover, the frequencies of f_2, f_3, and f_4 cannot be recognized by MWD in figures 3(b), (d) and (f). Furthermore, neither of the modulated features $(f_2 \pm f_1)$ can be clearly observed in figures 3(a)–(f). The results also indicate that the MWSD method has better performance than MWD.

Eventually, the proposed MMSTW with a thresholding technique is utilized to analyze the simulation signal, and the results are shown in figure 4. It is evident that both feature frequencies (f_2, f_3, and f_4) and modulated features $(f_2 \pm f_1)$ of the three sensors can be identified. Comparing figures 3 and 4, the proposed method exhibits an expected performance in multisensor signal noise reduction.

4. Experimental studies

4.1. Case 1: signal collected from a faulty rolling bearing system

To illustrate the effectiveness of the proposed method in practical applications, bearing failure data collected from a rolling bearing system was analyzed in this section. The schematic diagram is shown in figure 5. The apparatus includes two motors, and a coupling (containing a torque sensor and encoder). The test rig was equipped with a replaceable rolling bearing with the parameters as listed in table 1. The outer race of the rolling bearing was fabricated by using the electrical discharge machining method to simulate the failure of the outer race. The x, y, and z directions of the vibrational signal were collected by a three-axis acceleration sensor (PCB, America), which was placed on the measuring point. There were $n = 8$ roller elements in the bearing, the roller element diameter was $d = 11.11$ mm, and the contact angle was $\alpha = 0°$. Through theoretical calculation [32], the fault feature frequency of outer race was determined as $f_o = 80$ Hz.

The presentation of the originally measured vibration signal in the frequency domain is shown in figures 6(a), (c) and (e). It can be found that the fault feature frequency f_o and its multiple frequencies are interfered with by other signal components due to the system and environmental noises; this significantly influences the determination of the fault frequency. Similarly, the result computed by MWD is plotted in figures 6(b), (d) and (f). It can be found that the rotation frequency f_r and its multiple frequencies have been identified. However, the feature frequency of the outer race f_o still cannot be accurately extracted.

Subsequently, the original multivariate denoising algorithms based on MWSD were executed for experimental data analysis. The results are shown in figure 7. Similarly, only the rotation frequency f_r and its multiple frequencies are extracted. The outer race fault frequency cannot be found due to the interference of other signal components. Figure 8 gives the results, which are computed by using the MMSWT and the thresholding $T_{\mathrm{mod}} = 0.3$ under the condition of equation (15). The major difference between the MMSWT and MWSD is that the former employs a high-order chirp rate estimation, namely the matching synchrosqueezing transform. It is noted that figures 8(a)–(c) correspond to the frequency domain results of the three-axis sensor signal denoising performed by the MMSWT. From figure 8, it can be observed that the outer race fault frequency f_o and its multiple frequencies ($2f_o$, $3f_o$, $4f_o$, $5f_o$, and $6f_o$) can be obtained. The rotation frequency f_r can also be identified in the three-axis sensor signal. Most importantly, the noise components have already been removed. Thus, the performance of the proposed method on fault frequency extraction of rolling bearing systems is verified.

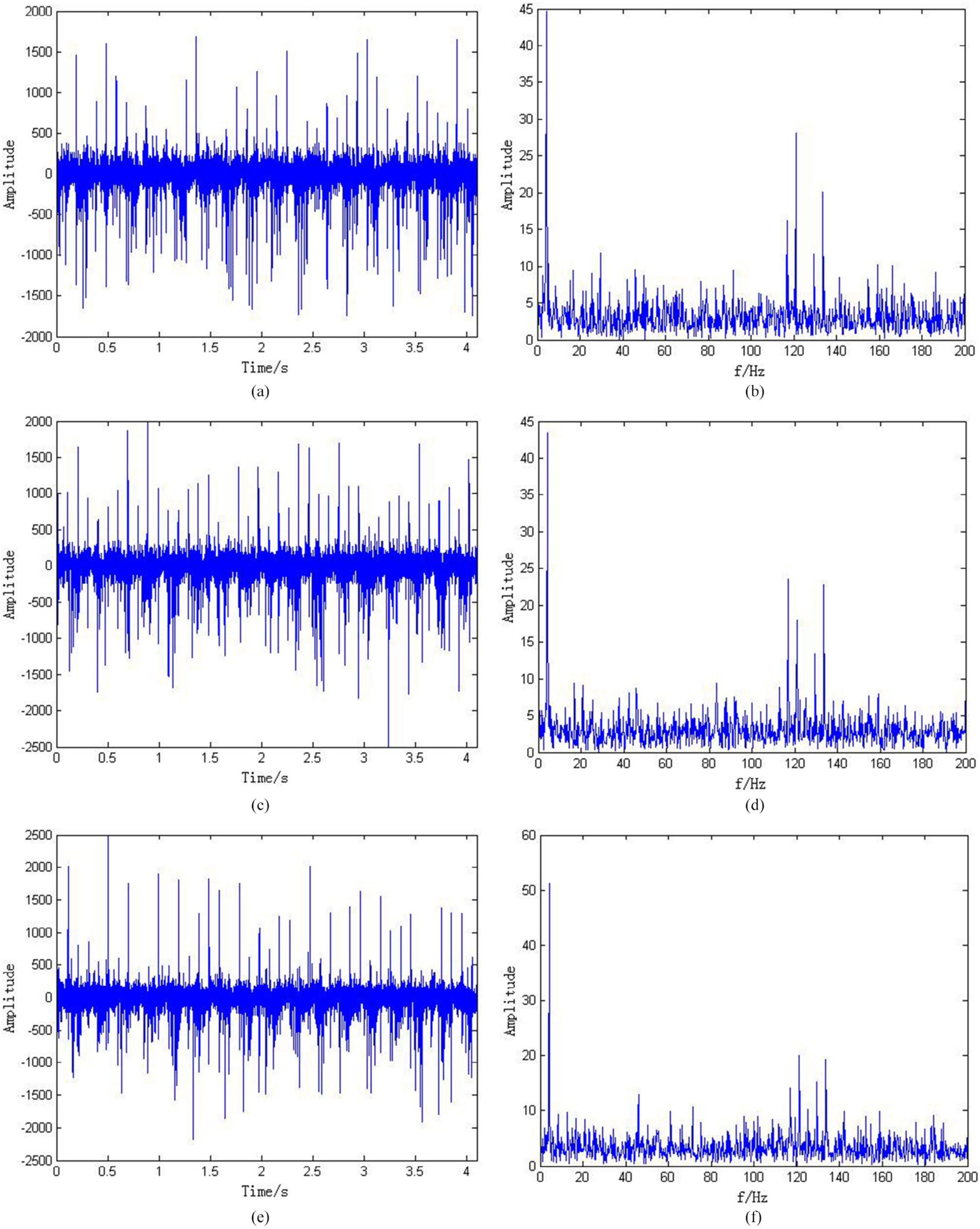

Figure 10. Time and frequency responses of faulty gear signal. (a) Fault gear signal of the *X*-scale in the time domain. (b) Fault gear signal of the *X*-scale in the frequency domain. (c) Fault gear signal of the *Y*-scale in the time domain. (d) Fault gear signal of the *Y*-scale in the frequency domain. (e) Fault gear signal of the *Z*-scale in the time domain. (f) Fault gear signal of the *Z*-scale in the frequency domain.

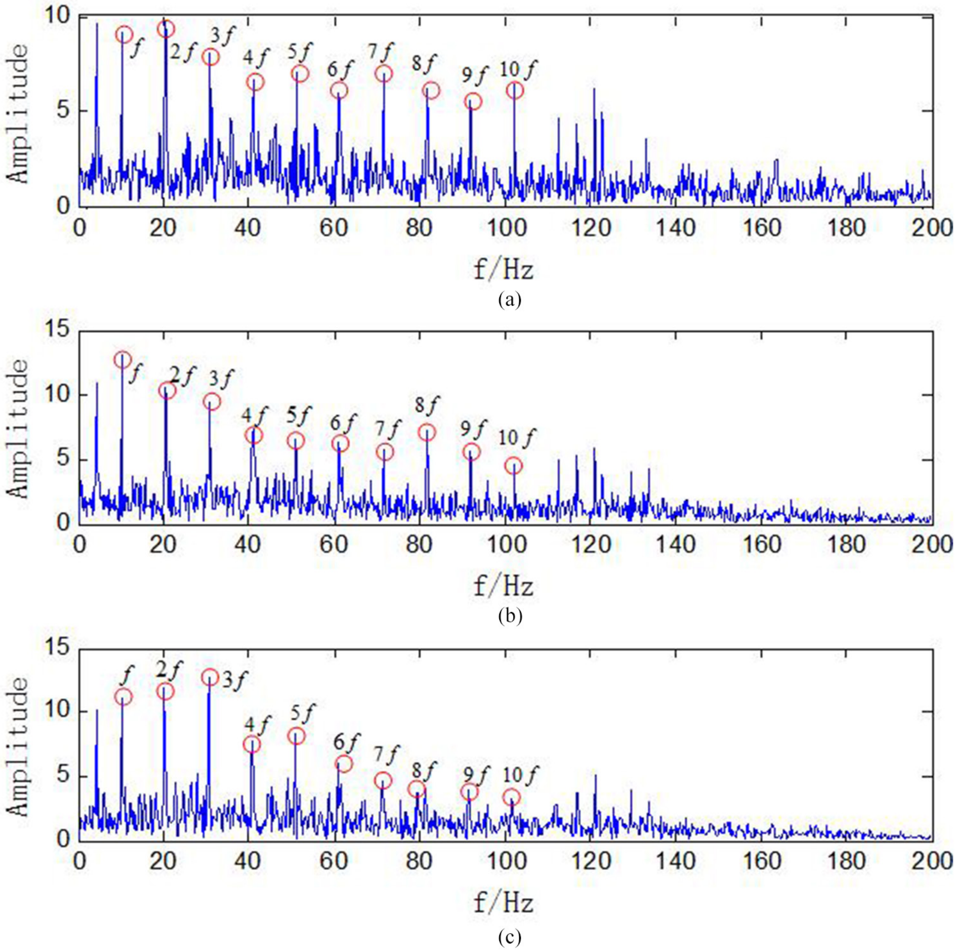

Figure 11. Results computed by the proposed method (MMSWT). (a) Denoised signal of the *X*-scale by the MMSWT. (b) Denoised signal of the *Y*-scale by the MMSWT. (c) Denoised signal of the *Z*-scale by the MMSWT.

4.2. Case 2: signal collected from a faulty gear system

Due to the unqualified manufacturing and improper processor manipulation, different kinds of gear faults occur during operation. In this section, the proposed MMSWT method is verified by the fault signal collected from a gear system, as shown in figure 9. The gear system includes a motor, a single-stage cylindrical gear reducer, and a magnetic powder brake. The whole device uses the first reduction gearbox for transmission, in which the small gear is mounted on the input shaft to drive the big gear installed on the output shaft. The teeth numbers of the small gear and big gear are $z_1 = 20$ and $z_2 = 37$, respectively. The transmission ratio is 1.85, and the module of gears is 3. The load is generated by the magnetic powder brake, and the three-direction acceleration sensor is installed on the bearing pedestal of the input shaft. The specific parameters of the test conditions are as follows: the speed of the high-speed axis in the experiment is 612 r min^{-1}, the sampling frequency is $f_s = 2000\,Hz$, and number of sampling points is $N = 8192$. In this study, one of the teeth in the small gear was broken, and the signal was measured by a three-axis acceleration sensor (PCB, America). According to the fault mechanism and fault characteristics of gears in [33], the calculated failure frequency of breaking a tooth is $f = 10.2$ Hz.

The time domain and frequency domain expressions of the faulty signal collected from the faulty gear system are shown in figure 10. The faulty signal includes a large amount of noise components, resulting in the failure to directly observe the fault information. As shown in the figure, the shock characteristic caused by the broken tooth of the investigated gear system is obvious. Figures 10(b), (d) and (f) present the results of frequency spectrum analysis performed by FFT, and the failure frequency f still cannot be extracted.

To reduce the interference of noise components, and retain the fault characteristic information, the improved algorithm MMSWT was employed to deal with the faulty gear signal. Figure 11 shows the results computed by the MMSWT, and the threshold is determined as $T_{\text{mod}} = 0.39$. It is seen that the failure frequency f and its multiple frequencies (from f to $10f$) can be clearly observed. Additionally, the results based on MWSD are drawn in figure 12. Unfortunately, the unique peak shown in figure 12 is corresponding to 4 Hz, which is unrelated to the failure feature frequency f. Thus, its performance is not acceptable. From the comparative results between figures 11 and 12, the effectiveness of the proposed MMSWT-based algorithm for fault diagnosis of gear systems can be verified.

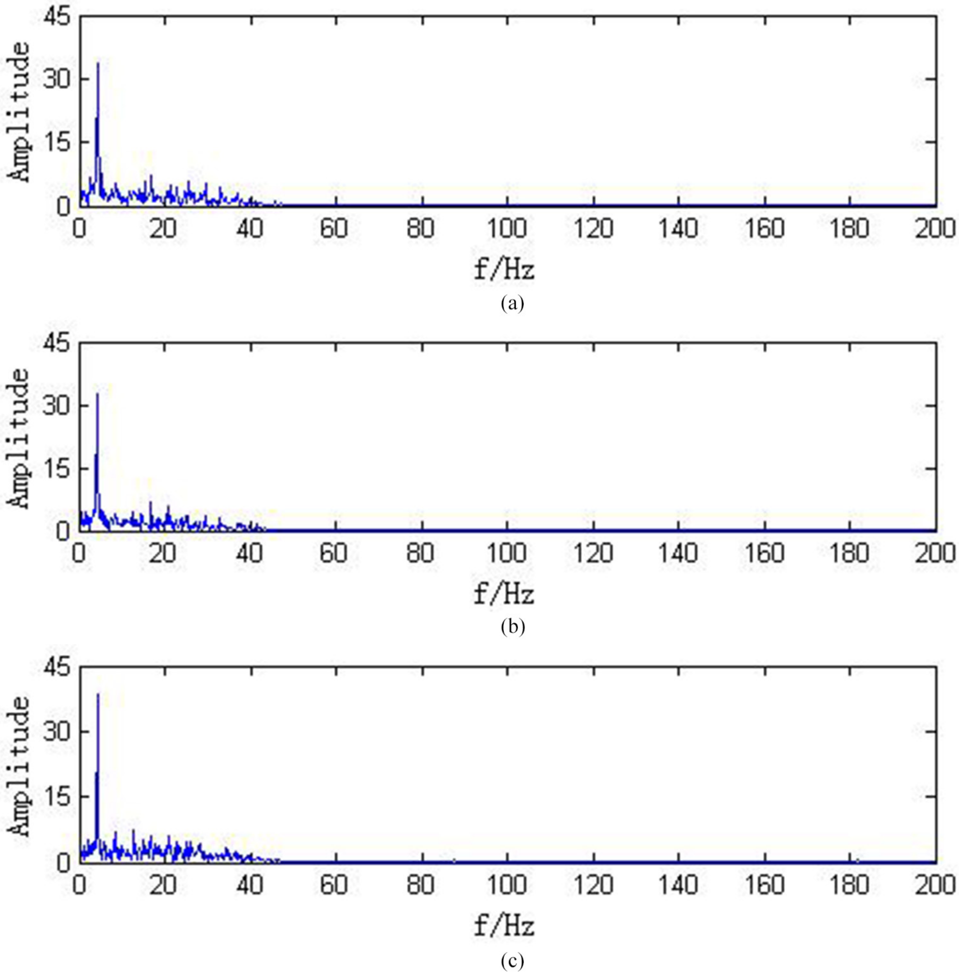

Figure 12. Results computed by MWSD. (a) Denoised signal of the *X*-scale by MWSD. (b) Denoised signal of the *Y*-scale by MWSD. (c) Denoised signal of the *Z*-scale by MWSD.

5. Conclusions

In this paper, a novel multisensor signal denoising algorithm based on the MSWT was proposed for fault feature identification. The main work of this paper includes the following aspects: (1) In order to improve the performance of denoising and signal resolution, the MSWT based on high-order chirp rate estimation was firstly introduced for fault condition assessment. (2) Based on the multivariate modulated oscillation model, the common modulated oscillations in multiple sensors and inter-sensor dependencies were captured. Then, the multisensor denoising algorithm MMSWT was studied. (3) The proposed method was illustrated by numerical analysis, as well as application to multisensor signal feature extraction of fault bearing and gear systems. The results demonstrated that the proposed method can provide improved performance of multisensor complex signal denoising.

Acknowledgments

This work was supported by the National Natural Science Foundation of China under Grant No. 51475339, the Natural Science Foundation of Hubei Province under Grant No. 2016CFA042, the Applied Basic Research Programs of Wuhan Science and Technology Bureau under Grant No. 2017010201010115, the Engineering Research Center for Metallurgical Automation and Measurement Technology of Ministry of Education (Wuhan University of Science and Technology) under Grant No. MARC201701, and Guangxi Key Laboratory of Optoelectronic Information Processing Open Foundation of China under Grant No. KFJJ2017-01.

ORCID iDs

Yong Lv https://orcid.org/0000-0002-5571-2043

References

[1] Gu X *et al* 2016 Rolling element bearing faults diagnosis based on kurtogram and frequency domain correlated kurtosis *Meas. Sci. Technol.* **27** 125019
[2] Yi C, Lv Y and Dang Z 2016 A fault diagnosis scheme for rolling bearing based on particle swarm optimization in variational mode decomposition *Shock Vib.* **2016** 9372691 (https://doi.org/10.1155/2016/9372691)
[3] Wang J Q *et al* 2016 Detrended fluctuation analysis and Hough transform based self-adaptation double-scale feature extraction of gear vibration signals *Shock Vib.* **2016** 3409897

[4] Wang P, Gao J and Wang Z 2014 Time-frequency analysis of seismic data using synchrosqueezing transform *IEEE Geosci. Remote Sens. Lett.* **11** 2042–4

[5] Flandrin P, Rilling G and Goncalves P 2004 Empirical mode decomposition as a filter bank *IEEE Signal Process. Lett.* **11** 112–4

[6] Feng Z, Chen X and Liang M 2015 Iterative generalized synchrosqueezing transform for fault diagnosis of wind turbine planetary gearbox under nonstationary conditions *Mech. Syst. Signal Process.* **52** 360–75

[7] Wu H T *et al* 2014 Using synchrosqueezing transform to discover breathing dynamics from ECG signals *Appl. Comput. Harmon. Anal.* **36** 354–9

[8] Wu Z and Huang N E 2009 Ensemble empirical mode decomposition: a noise-assisted data analysis method *Adv. Adapt. Data Anal.* **1** 1–41

[9] Yi C *et al* 2017 Research on the blind source separation method based on regenerated phase-shifted sinusoid-assisted EMD and its application in diagnosing rolling-bearing faults *Appl. Sci.* **7** 414

[10] Boashash B 1992 Estimating and interpreting the instantaneous frequency of a signal. II. Algorithms and applications *Proc. IEEE* **80** 540–68

[11] Griffin D and Lim J 1984 Signal estimation from modified short-time Fourier transform *IEEE Trans. Acoust. Speech Signal Process.* **32** 236–43

[12] Andreaus U *et al* 2017 Experimental damage evaluation of open and fatigue cracks of multi-cracked beams by using wavelet transform of static response via image analysis *Struct. Control Health Monit.* **24** e1902

[13] Fan X L, Kou K I and Liu M S 2017 Quaternion Wigner–Ville distribution associated with the linear canonical transforms *Signal Process.* **130** 129–41

[14] Daubechies I, Lu J and Wu H T 2011 Synchrosqueezed wavelet transforms: an empirical mode decomposition-like tool *Appl. Comput. Harmon. Anal.* **30** 243–61

[15] Auger F *et al* 2013 Time-frequency reassignment and synchrosqueezing: an overview *IEEE Signal Process. Mag.* **30** 32–41

[16] Li C and Liang M 2012 Time–frequency signal analysis for gearbox fault diagnosis using a generalized synchrosqueezing transform *Mech. Syst. Signal Process.* **26** 205–17

[17] Huang Z *et al* 2016 Synchrosqueezing S-transform and its application in seismic spectral decomposition *IEEE Trans. Geosci. Remote Sens.* **54** 817–25

[18] Oberlin T, Meignen S and Perrier V 2015 Second-order synchrosqueezing transform or invertible reassignment? Towards ideal time-frequency representations *IEEE Trans. Signal Process.* **63** 1335–44

[19] Yang H 2015 Synchrosqueezed wave packet transforms and diffeomorphism based spectral analysis for 1D general mode decompositions *Appl. Comput. Harmon. Anal.* **39** 33–66

[20] Wang S *et al* 2017 Matching synchrosqueezing wavelet transform and application to aeroengine vibration monitoring *IEEE Trans. Instrum. Meas.* **66** 360–72

[21] Aminghafari M, Cheze N and Poggi J M 2006 Multivariate denoising using wavelets and principal component analysis *Comput. Stat. Data Anal.* **50** 2381–98

[22] Rilling G *et al* 2007 Bivariate empirical mode decomposition *IEEE Signal Process. Lett.* **14** 936–9

[23] Rehman N and Mandic D P 2010 Empirical mode decomposition for trivariate signals *IEEE Trans. Signal Process.* **58** 1059–68

[24] Rehman N and Mandic D P 2010 Multivariate empirical mode decomposition *Proc. R. Soc.* **466** 1291–302

[25] Yi C *et al* 2017 Quaternion singular spectrum analysis using convex optimization and its application to fault diagnosis of rolling bearing *Measurement* **103** 321–32

[26] Ahrabian A and Mandic D P 2015 A class of multivariate denoising algorithms based on synchrosqueezing *IEEE Trans. Signal Process.* **63** 2196–208

[27] Ahrabian A *et al* 2015 Synchrosqueezing-based time-frequency analysis of multivariate data *Signal Process.* **106** 331–41

[28] Lilly J M and Olhede S C 2012 Analysis of modulated multivariate oscillations *IEEE Trans. Signal Process.* **60** 600–12

[29] Peng Z K, Tse P W and Chu F L 2005 A comparison study of improved Hilbert–Huang transform and wavelet transform: application to fault diagnosis for rolling bearing *Mech. Syst. Signal Process.* **19** 974–88

[30] Kopsinis Y and Mclaughlin S 2009 Development of EMD-based denoising methods inspired by wavelet thresholding *IEEE Trans. Signal Process.* **57** 1351–62

[31] Wang S *et al* 2018 Matching synchrosqueezing transform: a useful tool for characterizing signals with fast varying instantaneous frequency and application to machine fault diagnosis *Mech. Syst. Signal Process.* **100** 242–88

[32] Randall R B, Antoni J and Chobsaard S 2001 The relationship between spectral correlation and envelope analysis in the diagnostics of bearing faults and other cyclostationary machine signals *Mech. Syst. Signal Process.* **15** 945–62

[33] Mohammed O D *et al* 2013 Vibration signal analysis for gear fault diagnosis with various crack progression scenarios *Mech. Syst. Signal Process.* **41** 176–95